THE JOURNAL OF PHYSICAL CHEMISTRY C

Article

pubs.acs.org/JPCC

A Multipulse Time-Resolved Fluorescence Method for Probing Second-Order Recombination Dynamics in Colloidal Quantum Dots

Gaurav Singh,[†] Michael A. Guericke,[†] Qing Song,[‡] and Marcus Jones*[,†]

[†]Department of Chemistry, University of North Carolina at Charlotte, 9201 University City Boulevard, Charlotte, North Carolina 28223, United States

[‡]IBM Research Almaden, 650 Harry Road, San Jose, California 95120, United States

Supporting Information

ABSTRACT: The ability to generate and utilize multiexcited electronic states in colloidal quantum dots (QDs) is key to a growing range of QD technologies, but the factors that control their radiative and nonradiative recombination dynamics are not yet fully resolved. A significant barrier toward a greater understanding of these species is the fact that their spectroscopic signatures are energetically close to dominant exciton transitions, making it difficult to separate their decay contributions in inhomogeneously broadened ensembles. Here we describe a multipulse technique wherein a controllable number of 80 MHz laser pulses are used to generate different excited state populations, which are then monitored using time-resolved fluorescence. By changing the number of pulses and using a general data analysis method we are able to separate second-order emission generated by absorption of two or more laser pulses from first-order contributions generated by just one pulse. Furthermore, we show that it is possible to determine the nature of the multiexcited state by comparing the second-order emission intensity to models of QD decay dynamics. We find that in our sample of CdSe/CdS core/shell QDs the second-order emission is dominated by emissive trion states rather than biexcitons. Our spectroscopic technique offers a powerful new way to study multiexcited QDs, and the insights that will be gained from this and future studies could be an important step toward harnessing multiexcitons and other multiexcited states in new QD technologies.

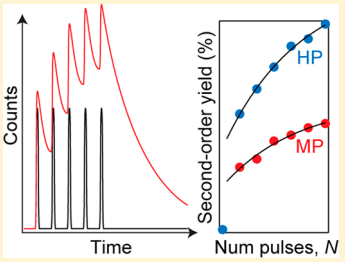

1. INTRODUCTION

Colloidal semiconductor quantum dots (QDs) have garnered tremendous scientific and technological interest due to their unique physical and chemical properties.[1,2] Their size-tunable optoelectronic properties and processability make them an exciting class of materials for a wide range of device applications.[3−10] The majority of studies on QD electronic properties has so far focused mostly on the photophysics of single exciton states, including their relaxation dynamics,[11−14] their coupling with phonon modes,[15−17] and their interaction with surface or ligand states.[18−21] However, experimental realization of multiexciton generation (MEG)[22−26] in QDs and the potential of MEG-based solar cells[27−30] to make a significant leap in photoconversion efficiency has garnered significant interest in the study of multiexciton states.[31−34] Multiexciton states are equally important for the practical realization of optical gain in QD-based lasers[35,36] or for using QDs as entangled photon sources.[37,38] On the other hand, nonradiative recombination of multiply excited states[39] is thought to play a key role in QD blinking and QD photocharging,[40,41] and its understanding has important implications for using QDs as reliable biomarkers,[42,43] bright light-emitting diodes (LEDs),[44] or single photon sources.[7,45]

Ultrafast transient absorption (TA) and time-resolved photoluminescence (TRPL) spectroscopy have been the mainstay techniques used to probe multiple exciton dynamics in QDs.[46−49] TA is a powerful technique that can have a very high temporal resolution, can be extended to very long lifetimes, and can probe any optically active transition, including, e.g., intraband relaxation dynamics in CdSe QDs.[50] It is typically a low repetition rate measurement (kHz) requiring relatively high excitation intensities, but much higher repetition rate experiments are also possible.[51] Recent work has extended TA studies to the study of single-particle ultrafast dynamics,[52] which is very challenging because it requires the determination of very small changes in probe-beam intensity.

Ultrafast TRPL has been used to study multiexciton dynamics of a few tens of picoseconds or less,[47] but the upconversion technique suffers from a restricted time window that makes it impractical to study most QD dynamics. Time-correlated single photon counting (TCSPC) is an alternative TRPL technique, which requires low light intensities, utilizes comparatively simple instrumentation, and is able to probe dynamics from tens of picoseconds to microseconds. It is a powerful tool for understanding QD carrier recombination dynamics;[53] however, the time resolution is not as short as TA, and in ensemble experiments, it is challenging to separate exciton luminescence from multi- or charged-exciton emission because their spectral shifts are often similar to the inhomogeneously broadened exciton line widths, making the

Received: May 4, 2014
Revised: June 13, 2014

 © XXXX American Chemical Society dx.doi.org/10.1021/jp5043766 | J. Phys. Chem. C XXXX, XXX, XXX−XXX

contributions of weakly emitting species hard to identify on top of an already complex multiexponential fluorescence decay.[54,55] For these reasons, ultrafast TA has most often been used to study multiexciton dynamics in colloidal QDs.

Long-lived photocharged QDs can be generated, especially at high photon energies, and their subsequent excitation can lead to trions and higher-order states with recombination dynamics similar to multiexcitons. As a result, these states have been a source of confusion for calculating the correct multiexciton quantum yields and associated spectroscopic signatures.[49,56−58] Multiple exciton emission can also be directly inferred by photon correlation measurements using single-molecule techniques;[59] however, these techniques are also vulnerable to photocharging and, ultimately, photobleaching. An ensemble fluorescence technique able to distinguish emission from charged QDs versus multiexcitons could therefore be an important addition to the field.

Under low excitation fluence, emission from CdSe core and core/shell quantum dots arises from thermally populated levels within the ground-state exciton manifold;[60] however, nonradiative transitions to and from surface- or ligand-localized states give rise to characteristically long multiexponential tails in all but the most highly fluorescent QDs.[61−65] At higher excitation intensities, CdSe QDs can absorb two photons to generate biexcitons, which can recombine radiatively, or nonradiatively, to form excitons. Auger ionization from biexcitons can also lead to the formation of charged QDs,[66] including trion states, which were formerly thought to be nonemissive[67] but are now considered to be weakly luminescent.[68,69]

Although Auger recombination adds an additional nonradiative decay pathway, recent work suggests that biexciton and trion lifetimes in some thick-shelled QDs are not substantially different from single exciton lifetimes.[59,70−72] This is thought to be due to different degrees of confinement experienced by the electrons and holes resulting in spatially separated wave functions. By steadily increasing laser fluence, previous ensemble TRPL studies of multiexcitons in CdSe QDs have identified fast *N*-exciton decay components whose amplitude increases with an *N*th-order dependence on laser fluence.[73] This approach works well when multiexcitons have reasonable emission yields and lifetimes that are somewhat shorter than excitons, but if the multiexcitons have low emission yields or recombination times comparable to lifetime components in single exciton decays it is very difficult to separate multiexciton from single exciton recombination dynamics.

Due to the difficulties encountered in studying multiexcited states in QDs, many of the factors that control their radiative and nonradiative recombination rates are poorly understood. It is increasingly important to improve our understanding as we learn how to put together increasingly complex devices that rely on multiexcitons to enhance their operation. An ensemble technique that is able to reliably distinguish multi- from single-excited states, even in the limit of low fluorescence yield, could therefore advance the field, enable us to learn much more about these states, and potentially help us design better ways of utilizing multiexcitons in new devices.

Time-resolved fluorescence is typically recorded using a pulsed light source wherein the pulse separation is significantly longer than the lifetime of the excited states. CdSe QD samples usually require pulse repetition rates of ∼1 MHz, or slower, to ensure that all the QDs are in their ground state before the next pulse arrives. If we want to study multiexcited QDs we have two choices: either increase the pump fluence or increase the pulse rate. The latter approach was recently considered by Saba et al.[74] In their work, a variable pulse rate source was used to investigate long-lived charged states in colloidal QDs; however, the decay window in their experiment was limited to ∼10 ns by the pulse separation at the highest repetition rates. Since this is much shorter than the emission time of the QDs it was consequently difficult to distinguish slower decay processes.

To overcome this issue we have taken a slightly different approach. Instead of illuminating our QDs with varying pulse repetition rate we have developed a gated time-correlated single photon counting experiment that excites the sample with a controllable number of 80 MHz laser pulses. In this article we describe the technique and demonstrate its efficacy using a sample of CdSe/CdS core/shell QDs. We show that our method can be used to clearly resolve both short and long decay components arising from multiexcited states that are distinct from the dynamics of singly excited QDs. Furthermore, we demonstrate that the long time window afforded by our gated technique allows us to distinguish neutral and charged multiexcited states, which could lead to significant advances in our understanding of QD fluorescence blinking.

2. METHODS

We utilized a procedure developed by Clapp et al.[75] to synthesize CdSe quantum dots. The detailed procedure can be found in a previous report.[19] A SILAR method first introduced by Li et al.[76] was then employed to grow CdS shells on as-prepared CdSe cores. This was achieved by alternatively injecting 0.1 M S-octadecene and Cd-oleate. The injections were preformed every 10 min, allowing 20 min for the growth and annealing of each monolayer. A spherical concentric shell model was utilized to calculate the amount of shell precursor required to grow each monolayer (ML).[77] The average thickness of one monolayer of CdS was taken as 0.35 nm, which is equal to half the *c*-lattice parameter of the bulk CdS. After the growth of each monolayer a small aliquot was taken out for optical measurements. The shell thickness of core−shell samples used in this study corresponds to 9.25 MLs of CdS. The resulting core−shell dots were then purified by precipitation with methanol. The washed core−shell samples were redispersed in hexane and stored under ambient conditions in the dark. Before use in these studies, the QD sample was degassed by several freeze−pump−thaw cycles to remove dissolved O_2.

A mode-locked femtosecond Ti:sapphire laser (Spectra Physics MaiTai), operating at 80 MHz repetition rate and 820 nm, was used as a synchronous pump source for an optical parametric oscillator (OPO) (Spectra Physics Inspire). The frequency-doubled output (410 nm) from the OPO was then directed through two electro-optic modulators (Conoptics 350-105 KD*P Series) driven by a high voltage push−pull power amplifier (Conoptics 25D). A delay generator (SRS DG535), externally triggered by a synchronous counter (Conoptics model 305) operating at 100 kHz, was used to produce an electronic gate of variable length which determined the length of the optical gate opened by the pulse-picker system. Varying the length of the electronic gate controlled the number of pulses in the sequence.

The pulse-picked frequency doubled light was then focused on a 10 mm quartz cuvette, containing the degassed QD sample, using a 500 mm uncoated plano-convex lens from

dx.doi.org/10.1021/jp5043766 | J. Phys. Chem. C XXXX, XXX, XXX−XXX

Newport. We collected the room-temperature sample fluorescence using the same lens, separated from the scattered laser light by a dichroic beam splitter (Semrock FF01-480) and a subtractive double monochromator (Spectral Products CM112). It was then detected by a hybrid PMT (Becker&Hickl HPM-100-40). Photon counting was done using Becker Hickl SPC-130 (short time window) and DPC-230 (long time window) counting modules.

Steady state emission was collected using a Jobin-Yvon Fluorolog 3 fluorimeter with a Hamamatsu R928 PMT detector. Absorbance measurements were made using a Cary 50 UV−vis spectrometer.

3. RESULTS AND DISCUSSION

Absorption and emission spectra for the CdSe/CdS core/shell QDs used in this study are shown in Figure 1a. The absorbance

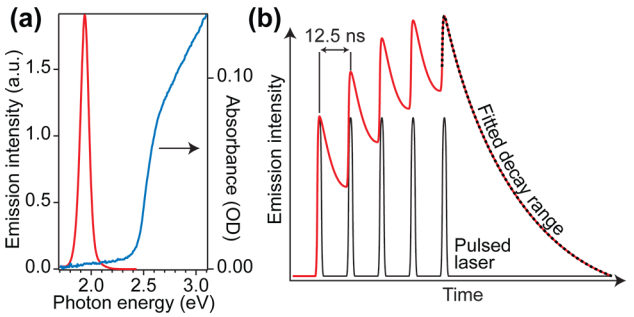

Figure 1. (a) Absorption and emission spectra of the CdSe/CdS QDs used in this study. (b) A schematic of the multipulse technique showing a 5-pulse experiment and analysis of the final pulse decay.

spectrum is characterized by a strong feature around 2.5 eV that is indicative of absorbance into the CdS shell. CdSe exciton states below this energy have a relatively low absorbance cross-section, and it is difficult to identify the lowest-energy exciton absorption peak. All the time-resolved experiments were run using 410 nm (3.02 eV) light, well above the CdS absorption threshold.

3.1. Multipulse Time-Resolved Fluorescence. The multipulse experiment we introduce in this article is outlined in Figure 1b. A controllably gated 80 MHz pulse sequence consisting of 1 to 25 pulses was generated using electro-optic modulators. The length of time between the start of two consecutive pulse sequences was held at 10 μs to give sufficient time for excited QDs to return to the ground state. Each pulse photoexcites a proportion of the QDs and generates a fluorescence decay that is added to any fluorescence generated by the previous pulses in the sequence. Composite plots containing seven representative PL data sets are presented in Figure 2a and b. These data were recorded using seven different pulse sequences (containing 1, 5, 9, 13, 17, 21, and 25 pulses) over a 500 ns and a 5 μs time window to ensure accurate determination of both short and long decay components. The final decay for each N-pulse pair (short and long time window) was simultaneously modeled with one multiexponential decay function convoluted with the measured 1-pulse instrument response function.[78]

Figure 2 shows that the peak intensities initially rise with N, reaching a quasi-equilibrium after approximately eight pulses (~100 ns). In other words, it takes about eight pulses for the exciton population lost to recombination to be balanced by the population generated each pulse. In addition, the decay shapes

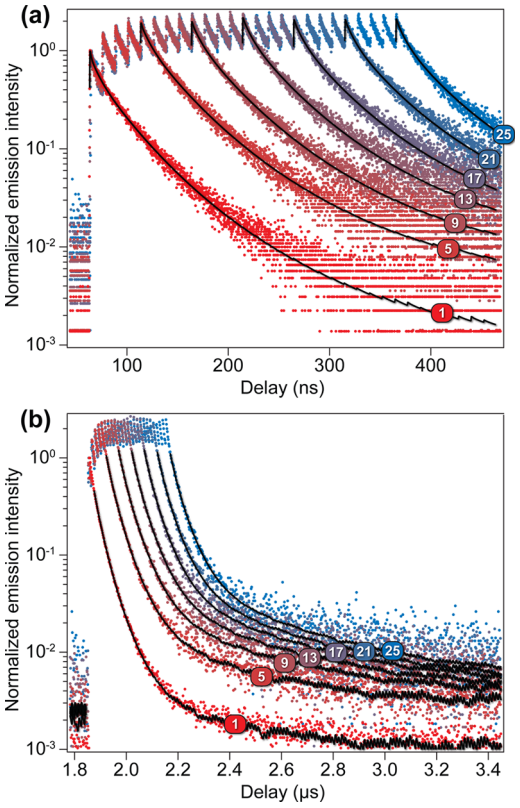

Figure 2. Composite plots of representative multipulse time-resolved fluorescence data recorded at low excitation power ($\lambda \sim 0.002$) over two different time windows: (a) 500 ns and (b) 5 μs. The number of laser pulses used to generate each of the decays is indicated. Black solid lines are the best multiexponential fits.

change slightly as a function of the number of laser pulses in the sequence, N. This is expected because each laser pulse in a sequence generates a decay that adds to and is offset from the previous decay. We can easily model how the decays change with N in the limit of very low excitation pulse energy. In these conditions, the chance of a QD absorbing more than one photon during the N-pulse series is negligibly small, so each pulse generates independent and identical fluorescence decays. The Nth pulse decay can then be represented as the sum of N successive decays, each offset by a time, Δt, corresponding to the interpulse period (12.5 ns in our experiment).

A typical 1-pulse QD fluorescence decay can be modeled with a multiexponential function, $I_1(t)$

$$I_1(t) = \sum_i \alpha_i e^{-k_i t} \tag{1}$$

If N pulses are used to excite the sample, then, in the limit of low fluence, the Nth decay can be generated using the same α and k parameters used to fit a 1-pulse decay

$$I_N(t) = \sum_{j=0}^{N-1} I_1(t + j\Delta t) = \sum_i \alpha_i e^{-k_i t} \sum_{j=0}^{N-1} e^{-jk_i \Delta t}$$

$$= \sum_i \alpha_i \left(\frac{1 - e^{-Nk_i \Delta t}}{1 - e^{-k_i \Delta t}} \right) e^{-k_i t} \tag{2}$$

This expression assumes an invariant ground-state population, but at higher excitation fluence the ground-state population will deplete steadily during the pulse sequence

dx.doi.org/10.1021/jp5043766 | J. Phys. Chem. C XXXX, XXX, XXX−XXX

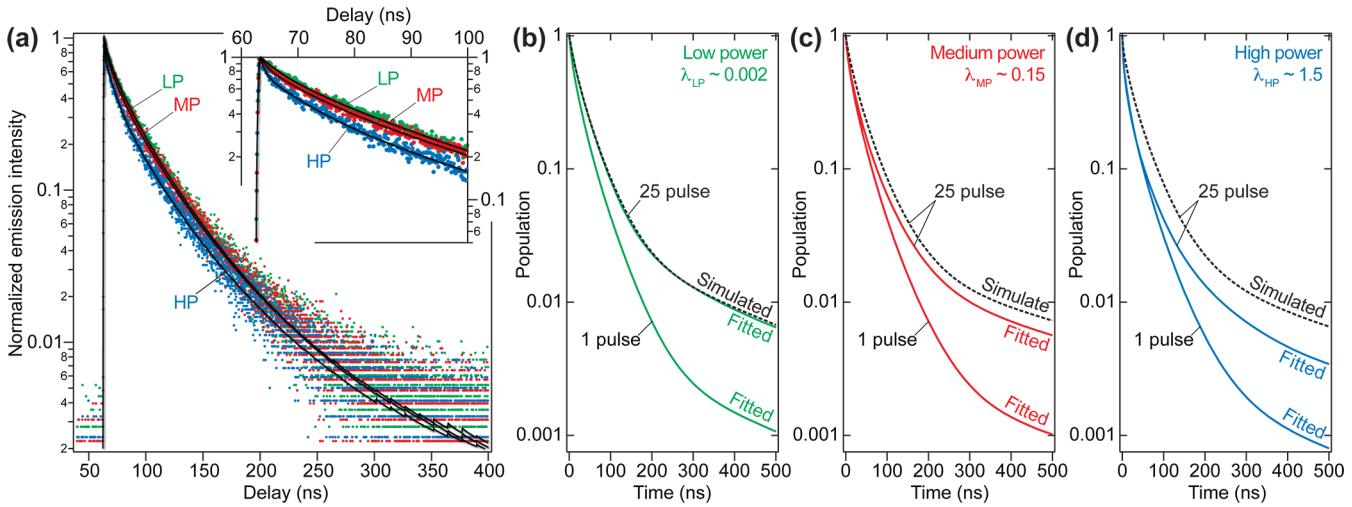

Figure 3. (a) One-pulse fluorescence decays recorded at low, medium, and high power and fit to multiexponential decay functions (black lines). The early parts of the decays are expanded in the inset plot. (b)−(d) Multiexponential decays extracted from fits to $N = 1$ ($I_1(t)$) and $N = 25$ ($I_{25}(t)$) TRPL decays recorded at (b) low (green curves), (c) medium (red curves), and (d) high power (blue curves). In each case the black dashed line is generated from $I_1(t)$ using eq 2.

(by up to 78% per pulse at the highest laser fluence used in these experiments); however, simulation of decay curves at the laser powers used in this article reveals that eq 2 remains a good approximation of the shape of the Nth decay. Details of this analysis are presented in the Supporting Information (S1).

In general, if an N-pulse QD fluorescence decay can be modeled with eq 2, using the α_i and k_i coefficients obtained after fitting a 1-pulse decay, it is a strong indication that the same distribution of excited states was formed after each pulse in the N-pulse experiment. Conversely, if eq 2 does not model the Nth decay when the α_i and k_i coefficients from a 1-pulse fit are used, it means that the second and subsequent laser pulses gave rise to a modified distribution of excited states with different fluorescence decay dynamics.

There are two possible explanations for the modified dynamics in QDs: (i) After their initial photoexcitation, some QDs could be photoexcited by a second pulse before relaxing to the ground state, leading to the formation of a subpopulation of emissive multiexcited QDs with different recombination dynamics to the QD population produced in the 1-pulse experiment. Alternatively (ii) if the sample contains QDs with widely varying decay dynamics, the multipulse experiment could bias the ensemble response toward the subpopulation of dots with more rapid recombination rates that have already returned to the ground state and are ready to be re-excited before the next pulse arrives.

Although the explanation (ii) could explain modified emission dynamics in our QDs, the degree of sample inhomogeneity would need to be quite large with a wide range of recombination times in the first ∼50 ns. This is not bourn out in the analysis of 1-pulse decays. Furthermore, our later discussion of Nth pulse emission intensities further reinforces our confidence that explanation (i) is most applicable to these QD systems. We shall, therefore, continue our discussion in the context of multiexcited QDs and briefly mention explanation (ii) toward the end of the article.

3.2. Experimental Conditions. Using estimated absorption cross sections we calculated the average number of excitation events per laser pulse, denoted λ.[70,79,80] A full description of this process is given in the Supporting Information (S2). Decay series were then recorded at three different average laser powers: low power (LP) = 7.46 nW, medium power (MP) = 560 nW, and high power (HP) = 5.6 μW, which corresponded to λ = 0.002, 0.15, and 1.5, respectively. Each series was recorded with N = 1, 5, 9, 13, 17, 21, and 25 pulses. The final decay in each series was then independently modeled with multiexponential decay functions (eq 1).

Plotted in Figure 3a are fitted 1-pulse fluorescence decays recorded at low, medium, and high laser powers. The medium power fluorescence decays slightly faster than the low power fluorescence at early times (shown inset), and the high power fluorescence decays even more rapidly. In both cases, deviations from the low intensity transient arise in the first few nanoseconds, which is consistent with the generation of a rapidly decaying multiexcited state after absorption of two or more photons during a single laser pulse.[73]

To gauge the likelihood of multiphoton absorption for N pulse experiments, we undertook an analysis of the excitation statistics, which is presented in the Supporting Information (S3). Assuming identical absorption cross sections for first, second, third, etc. excitations, the likelihood that a QD absorbs two or more photons in a single laser pulse is negligible (2×10^{-6}) at low power, small (0.01) at medium power, and quite likely (0.44) at high power, in qualitative agreement with the power-dependent appearance of a fast decay contribution in Figure 3a. Extending the analysis to 25 laser pulses, the chance that two or more photons are absorbed over the entire pulse sequence is still very low (0.0012) at low power but high for both medium (0.89) and high (1.00) power experiments.

There are two ways that a QD can absorb more than one photon during a 25 pulse sequence: either by absorbing multiple photons in a single pulse or by absorbing one photon during multiple pulses. Of course, both possibilities can occur within the same pulse sequence, but if we consider the probability that only the latter can occur (i.e., one photon from multiple pulses) we find that it is relatively high at medium power (0.66) but is negligible at low (0.0012) power and also at high power (5×10^{-7}) where there is, instead, a near-unity

dx.doi.org/10.1021/jp5043766 | J. Phys. Chem. C XXXX, XXX, XXX−XXX

likelihood that multiple photons are absorbed per pulse for at least one of the 25 pulses.

This statistical analysis highlights the difference between the medium and high power experiments: the medium power level was chosen to ensure predominantly single photon absorption per pulse, even over 25 laser pulses, whereas the high power level was chosen so that multiphoton absorption was likely each pulse. As we explain below, the relative powers give us a way to distinguish the two explanations for modified multipulse dynamics that we outlined above.

In Figure 3b–d we have plotted the $N = 1$ and $N = 25$ decay functions (solid lines) obtained by fitting multiexponential decay functions to the low, medium, and high power decays. Also plotted in Figure 3b–d are simulated decay functions, $I_{25}(t)$, (dashed lines) which were derived from the $N = 1$ multiexponential fits in the low power limit using eq 2.

At the lowest excitation power (Figure 3b) the simulated 25-pulse decay (dashed line) closely matches the fitted $N = 25$ decay (green curve), which is expected from the low likelihood (0.001) that an excited QD would absorb a second photon a low laser powers. However, at medium and high excitation intensities (Figure 3c and d), the simulated 25-pulse decays increasingly diverge from the fitted decay curves (red and blue), indicating that the recombination dynamics due to the second and subsequent pulses are different from the 1-pulse dynamics.

3.3. Decay Analysis. A fluorescence decay, $I_N(t)$, recorded after N laser pulses, can be separated into a series of distinct contributions. We will denote these contributions, $I_N^{(m)}(t)$ depending on how many separate laser pulses, m, contributed to the generation of the emitting state. For low excitation fluence, or slow pulse repetition rate, or if the quantum yield of second-order states is very low, then $I_N(t) \approx I_N^{(1)}(t)$ and we can use eq 2 to model N pulse decays (Figure 3b).

If, however, two or more pulses occur within the QD's exciton lifetime then, assuming sufficient laser fluence and measurable fluorescence intensity from multiexcited states, higher-order decay terms will contribute to the N-pulse decay and $I_N(t) = \sum_{m=1}^{N} I_N^{(m)}(t)$. For example, second-order fluorescence can arise from QDs that have absorbed a photon from pulse i and then absorb a second photon from pulse j ($i \neq j$) within the exciton lifetime. In an N-pulse sequence these decay contributions will be denoted, $I_N^{(2)}(t)$. Notice that $I_N^{(2)}(t)$ contributions are second-order with respect to the number of laser pulses but not necessarily with respect to the number of photons per pulse. This is because QDs that absorb two photons after interacting with just one laser pulse still contribute to $I_N^{(1)}(t)$, whereas only the fluorescence that arises after interaction with two *separate* pulses contributes to $I_N^{(2)}(t)$.

Since it takes at least m pulses to observe the contribution of the m^{th}-order term we can, in general, generate the $I_N^{(m)}(t)$ decay contribution from $I_m^{(m)}(t)$ using a modified version of eq 2

$$I_N^{(m)}(t) = \sum_{j=0}^{N-m} I_m^{(m)}(t + j\Delta t) = \sum_i \alpha_{i,m}\left(\frac{i - e^{-(N-m+1)k_{i,m}\Delta t}}{1 - e^{-k_{i,m}\Delta t}}\right)e^{-k_i t} \quad (3)$$

where $\alpha_{i,m}$ and $k_{i,m}$ are the ith pre-exponential coefficient and decay constant for the $I_m^{(m)}(t)$ decay.

Using eq 3 we defined a fit function, $I_N(t)$, based on just first- and second-order contributions that we used to fit our N-pulse decays

$$I_N(t) = \chi_N^{(1)} I_N^{(1)}(t) + \chi_N^{(2)} I_N^{(2)}(t) \quad (4)$$

where the relative weighting of first- and second-order contributions in each of the N-pulse decays was determined by the fitting parameters, $\chi_N^{(m)}$, and each $I_N^{(1)}(t)$ and $I_N^{(2)}(t)$ contribution was calculated from $I_1^{(1)}(t)$ and $I_2^{(2)}(t)$, respectively, using eq 3. Note that second-order contributions are, by definition, absent from the 1-pulse experiments so $\chi_1^{(2)} = 0$.

Using eq 4 we were able to simultaneously model the final decay from each pulse series ($N = 1$, 5, 8, 13, 17, 21, and 25). Medium and high power data were modeled using two decay functions, $I_1^{(1)}(t)$ and $I_2^{(2)}(t)$, combined with a pair of weighting parameters, $\chi_N^{(1)}$ and $\chi_N^{(2)}$, for each data set. Low power decays were recorded in the single excitation regime (Figure 3b), and these data could be fit simultaneously using a first-order model with $\chi_N^{(2)} = 0$.

In total, 14 decays (short and long time windows for each N) were globally fit for low, medium, and high power experiments. The low power data were fit using using 7 decay constants; 6 pre-exponential coefficients (α_1 was set to 1 and held constant); 14 pump shift parameters (accounting for instrumental deviations in the timing of decay and instrument response data); 13 scaling parameters (accounting for the different number of counts in the peak channel relative to the first decay); and 7 values of $\chi_N^{(1)}$, making a total of 47 independent parameters, or a little over 3 per decay. Note that seven exponentials were the minimum required to achieve an acceptable fit: reduced chi-squared, $\chi^2 < 1.1$, and Durbin–Watson parameter, $|d - 2| < 0.05$. Although 47 parameters seems like a lot, it is significantly fewer than the 119 that would have been required to analyze each of the 7 decay pairs independently.

Fits to the medium and high power decays required a second-order contribution, $I_N^{(2)}(t)$, to account for modified recombination dynamics with increasing N. $I_2^{(2)}(t)$ was found to be a single exponential decay function for the medium power fluorescence and a biexponential function for the high power data. The extra contribution brought the total number of independent fit parameters to 54 for both powers, nearly 4 per data set (one fewer exponential component was required to fit the first-order contributions for the high power decays). Note that although we could not rule out the contribution of third-order dynamics, our decay analysis suggests that their contribution is likely $\ll$1% of the total yield. In future experiments we plan to automate the collection of N-pulse data, allowing for longer collection times, a greater pulse range, and better signal-to-noise, which should enable us to identify higher-order contributions if they exist.

3.4. Analysis of Recombination Dynamics. *Average Emission Times.* Average, intensity-weighted, fluorescence lifetimes (integrated over a 1 μs time window[61]) for the first- and second-order decay contributions, $I_1^{(1)}$ and $I_2^{(2)}$, are presented in Table 1. Notably, second-order emission times were considerably faster than the first-order lifetimes as expected from multiexcited states with fast Auger recombination pathways.

Total average decay times, τ_{I_N}, were calculated from $I_N(t)$ (eq 4) and are presented in Figure 4a. The $N = 1$ data points are the average emission times of the first-order decay contributions given in Table 1 and show a slight increasing trend with laser power. However, due to the increasing contribution of fast second-order processes, $I_2^{(2)}(t)$, the average lifetimes for $N > 1$ show the opposite trend. In Figure 3a, it appears that the high

dx.doi.org/10.1021/jp5043766 | J. Phys. Chem. C XXXX, XXX, XXX–XXX

Table 1. First- and Second-Order Average Intensity Weighted Emission Lifetimes for Low, Medium, and High Power Experiments[a]

λ^b	$\langle\tau_{I_1^{(1)}}\rangle^c$	$\langle\tau_{I_1^{(2)}}\rangle^c$
$0.002 \pm 7 \times 10^{-4}$	48.8 ± 0.1	-
0.15 ± 0.054	51.4 ± 0.1	8.0 ± 0.3
1.5 ± 0.54	53.2 ± 0.2	6.7 ± 0.2

[a]Estimated lifetime uncertainties were determined using a procedure described in the Supporting Information (S4). [b]Average number of excitation events per laser pulse. [c]Average emission lifetimes (nanoseconds).

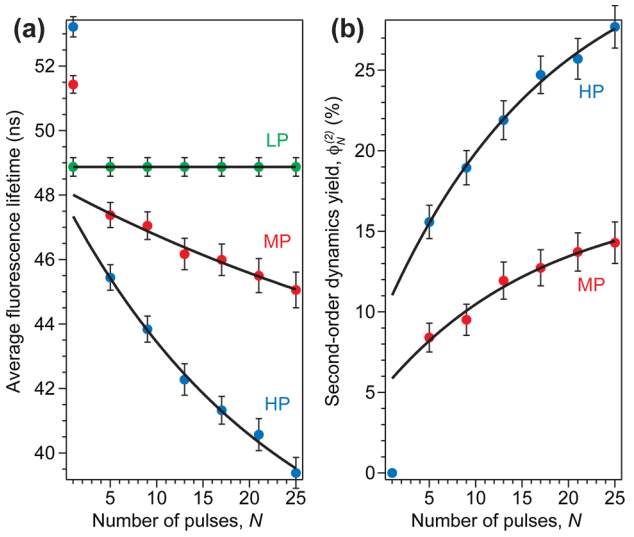

Figure 4. (a) Average fluorescence lifetimes and (b) second-order percentage yields, $\phi_N^{(2)}$, after N laser pulses. In each case, the error bars are ±2 × the standard deviation.

power 1-pulse decay is shorter that the other two; however, a slightly longer microsecond tail, presumably due to carrier trapping, gives rise to slower average recombination times. If the process that gives rise to this long tail arises from multiphoton absorption, it should also contribute to second-order dynamics; however, due to difficulties in distinguishing small differences in long decay tails,[81] we were not able to assign any slow dynamics to the second-order component. The decay functions are fully tabulated in the Supporting Information (S5).

Second-Order Emission Yields. The percentage yields, $\phi_N^{(2)}$, of the second-order decay contributions after the Nth laser pulse were calculated using eq 5.

$$\phi_N^{(2)} = 100 \times \frac{\int_0^\infty \chi_N^{(2)} I_N^{(2)}(t)\mathrm{d}t}{\int_0^\infty I_N(t)\mathrm{d}t} \tag{5}$$

At both medium and high powers, $\phi_N^{(2)}$ is well modeled by an exponential function (Figure 4b)

$$\phi_N^{(2)} = \phi_\infty^{(2)} - \alpha e^{-\beta N} \tag{6}$$

$\phi_\infty^{(2)}$ is the second-order yield in the limit of an infinite number of pulses, and $\phi_\infty^{(2)}$ = 0.17 and 0.34 for medium and high power, respectively. The rate constant, β, is almost identical for medium (0.057 pulse^{-1}) and high power (0.056 pulse^{-1}) curves, suggesting that identical multiexcited states are being created in both experiments. These values of β also indicate that a quasi-equilibrium of second-order emission will be reached in ~40 pulses (500 ns).

This is considerably longer than the time it takes for the first-order dynamics to reach equilibrium (~8 pulses or ~100 ns), which suggests that second-order populations exist for considerably longer than excitons; however, this is at odds with the average (<10 ns) second-order PL lifetimes shown in Table 1.

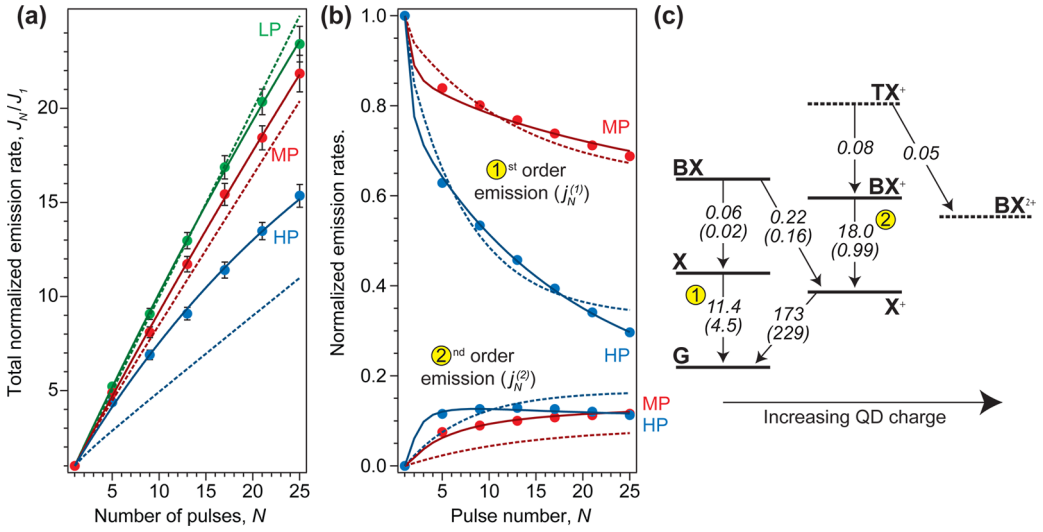

Figure 5. (a) Total normalized emission intensities, J_N/J_1, for low (green), medium (red), and high power (blue) experiments. Solid lines are exponential fits, and the dashed line is $J_N/J_1 = N$. Uncertainties are ±1σ and are estimated from the Poisson statistics associated with single photon counting experiments. (b) Normalized first- and second-order emission intensities after the Nth laser pulse, $j_N^{(1)}$ and $j_N^{(2)}$, for medium (red) and high power (blue) data sets. Fitted curves correspond to exciton and trion populations from fitting the five- (dashed curves) and seven-state (solid curves) schemes shown in (c). (c) Kinetic schemes used to model the $j_N^{(1)}$ and $j_N^{(2)}$ data in (b). The five-state scheme is shown (solid lines) with corresponding best-fit transition times (in ns) in parentheses. The seven-state scheme adds two more states (dashed lines), and the corresponding transition times are shown without parentheses. The transitions corresponding to first- and second-order emission are indicated.

dx.doi.org/10.1021/jp5043766 | J. Phys. Chem. C XXXX, XXX, XXX−XXX

The CdSe/CdS QDs used in this study had thick (9.25 monolayers) CdS shells, which were expected to reduce electron−hole coupling, slow Auger recombination rates,[33] and thereby increase the likelihood of second-order fluorescence; however, their relatively low emission yields (~20%) indicated that surface trapping and other nonradiative recombination pathways were active. Biexcitons are formed in CdSe/CdS QDs after absorption of two photons, and they can recombine to form (i) excitons (radiatively or nonradiatively) or (ii) charged states via Auger-induced ejection of an electron or hole.[66,68,82,83] Process (i) would explain the short second-order decay lifetimes, but simple carrier recombination does not explain the slow rise in second-order emission yield. Alternatively, a charged QD, formed via process (ii), could absorb another photon to give a trion, which also has a relatively short emission rate; however, the state formed after trion decay is the charged state, not the neutral ground state, and therefore, recovery of first-order dynamics requires that the QD discharges. If the ejected carrier is localized in a deep trap, the discharging time can be microseconds or longer,[21] as evidenced by QD "off" time fluorescence blinking statistics.[40,84] Since the emission yield from process (ii) could build up from pulse to pulse as more charged QDs are generated, these data suggest that trion emission rather than biexciton emission is responsible for the second-order dynamics in these QDs.

Let us return for a moment to the alternative explanation for second-order emission that we introduced earlier, namely, a re-excitation of QDs that have decayed to the ground state in <12.5 ns. If this process were solely responsible then we would expect that $\phi_N^{(2)}$ would equilibrate a little faster than the first-order exciton emission, i.e., in less than ~8 pulses. Since it actually takes ~40 pulses for $\phi_N^{(2)}$ to stop increasing, we can say with confidence that multiexcited QDs, not fast-recombining excitons, are responsible for the observed second-order emission.

Emission Intensities. We can further examine this model by considering the relative emission intensities of first- and second-order fluorescence contributions. Shown in Figure 5a are the total count rates, J_N, for each multipulse experiment (5 μs window, Figure 2b) normalized by the count rate for the N = 1 experiment, J_1. These were calculated by summing every channel in the photon counting data, subtracting the mean background count × the number of channels, correcting for the optical density of filters in the emission path, dividing by the time taken to record the data, and finally, dividing by the total count rate for the 1-pulse decay.

At first, the low power relative emission intensities (green dots) are equal to the number of pulses, as expected from a low excitation probability. After about 17 pulses, however, the low power intensities start to rise more slowly. This is likely due to a growing population of long-lived nonemissive trap states. More significantly, the medium and high power intensities (red and blue dots) increase sublinearly. This is likely due to saturation of the exciton transition (ground state depletion), as expected if a significant proportion of QDs are excited per pulse.

To get a more revealing picture of the excited state dynamics we decomposed the total intensities, J_N, into the relative emission intensities after the Nth laser pulse, denoted j_N, where $j_N = (J_N - J_{N-1})/J_1$. The $(J_N - J_{N-1})$ values were calculated from the best exponential fits to the total emission intensities in Figure 5a (black lines). The proportion of j_N due to first- and second-order emission, $j_N^{(1)}$ and $j_N^{(2)}$, was then calculated by multiplying j_N by $1 - \phi_N^{(2)}$ and $\phi_N^{(2)}$, respectively, where $\phi_N^{(2)}$ was extrapolated from the exponential fits in Figure 4b.

The $j_N^{(1)}$ and $j_N^{(2)}$ intensity curves for every fourth pulse are plotted for medium and high power regimes (red and blue markers, respectively) in Figure 5b. These data reveal that the drop in fluorescence intensity with increasing N at medium and high excitation powers (Figure 5a) is almost entirely due to declining first-order emission. In fact, the amount of second-order emission tends to increase with N, and although it starts to fall again in the high power experiment it is clear that the N-dependent intensity dynamics of first- and second-order emission contributions are quite different.

These emission intensity dynamics were analyzed using software previously developed for the analysis of time-resolved fluorescence decays.[61] This software enables the user to build an arbitrary first-order kinetic scheme, set initial populations, and propagate the dynamics over a predefined time interval. Using a global fitting routine, we modeled all the medium and high power intensity data in Figure 5b using the following procedure:

(i) Build a kinetic scheme, such as shown in Figure 5c, with initial population entirely in the ground state. Identify the transitions that will be assigned to first- and second-order emission.
(ii) Determine state populations after photoexcitation by using Poisson statistics and two adjustable expectation values, λ_{MP} and λ_{HP} (assuming the same absorption cross section for each vertical transition).
(iii) Propagate the dynamics for 12.5 ns or, if this is the Nth pulse in an N-pulse sequence, for ~200 ns to allow all the population to return to the ground state.
(iv) If there are remaining pulses, return to (ii); otherwise, find the total occupation probability of first- and second-order emitting states by integrating their final-pulse population decays.
(v) Repeat for other values of N and normalize all the total population probabilities to those determined for N = 1.
(vi) Compare the calculated populations with the $j_N^{(1)}$ and $j_N^{(2)}$ data for medium and high power experiments and adjust the kinetic model until a best fit is obtained.

Using this procedure, three kinetic schemes were tested. The first was a simple three-state scheme consisting of a ground state (G), exciton (X), and biexciton (BX), but, as already anticipated from the yield data in Figure 4b, this scheme was unable to model the $j_N^{(1)}$ and $j_N^{(2)}$ data with realistic transition rates because the biexciton rapidly recombines making it impossible to reproduce the relatively slow rise in second-order emission.

We then added an Auger ionization pathway from the biexciton, creating a charged exciton (X^+) that could be subsequently photoexcited to yield a trion (BX^+). This 5-state scheme is shown in Figure 5c (solid lines). The first- and second-order emission was designated to arise from X and BX^+ states, respectively. Using this scheme we obtained somewhat reasonable fits to $j_N^{(1)}$ and $j_N^{(2)}$ data for medium and high power experiments (dashed curves in Figure 5b). Transition times for the best-fit 5-state scheme are indicated in parentheses in Figure 5c and are broadly reasonable; however, the excitation parameters obtained for the 5-state scheme were λ_{MP} = 0.95 and λ_{HP} = 3.42, which are significantly higher than the experimentally measured values (λ_{MP} = 0.15 and λ_{HP} = 1.5).

dx.doi.org/10.1021/jp5043766 | J. Phys. Chem. C XXXX, XXX, XXX−XXX

Note that positive charging has been assumed in our notation since, in CdSe/CdS QDs, the hole wave function is localized in the core, whereas that of the electron is delocalized over the entire structure.[85,86] It is therefore likely that trions form after reversible electron trapping in surface states; however, in these experiments we were not able to distinguish the type of trion being formed.

In an attempt to further improve the fits we added a second Auger ionization step from charged triexciton (TX^+) to doubly charged biexciton (BX^{2+}). This scheme immediately yielded much better fits (solid curves in Figure 5b), accounting for all the trends, including the drop in second-order emission at high power after ~13 pulses. The best-fit transition times for this scheme are shown in Figure 5c without parentheses and are broadly in line with what we would expect: sub-100 ps multiexciton lifetimes, exciton recombination around 10 ns, and discharging times in the hundreds of nanoseconds. In addition, the excitation parameters were λ_{MP} = 0.31 and λ_{HP} = 0.72, much closer to the measured values than for the 5-state scheme. A complete tabulated list of the 5- and 7-state fit parameters, together with estimated uncertainties, is presented in the Supporting Information (S6).

One surprise from the 7-state fit was the long trion lifetime; however, we note that despite their apparent complexity these kinetic schemes still predict single exponential first-order decay dynamics because they ignore carrier trapping and exciton fine structure, which have been shown to yield multiexponential decays.[21] Furthermore, exciton and biexciton absorption cross sections are known to differ markedly, especially at higher excitation energies due to a higher density of biexciton states.[87] This means that the assumption of equal absorption cross sections is likely not very good. Nevertheless, this analysis strongly suggests that second-order emission in these QDs comes from trions and, perhaps, higher-order charged states rather than neutral biexcitons.

So, why did we not observe biexciton emission in these QDs? In spite of a relatively thick CdS shell, emission efficiencies were poor (~20%) indicating a significant population of surface defects or trap states that could increase the rate of biexciton Auger ionization, making radiative recombination less likely. Furthermore, a significant density of CdS valence band states, associated with the shell, could have provided an efficient pathway for biexciton Auger recombination wherein a hole is excited deep into the valence band after recombination of an electron−hole pair. In the trion, we would expect Auger recombination to be statistically slower since there are eight ways for an electron−hole pair to recombine and give the excess energy to another carrier in a biexciton but only two ways in a trion. Furthermore, if negative rather than positive trions are being generated the lower density of states in the conduction band could also limit the rate of Auger recombination and promote radiative recombination of the trion.[88]

Previous work has shown that biexcitons as well as positive and negative trions can be spectrally separated.[72,88] In our studies we were unable to do this using steady state emission spectroscopy, but it should be possible, in follow-up work, to determine the spectral dependence of $\phi_N^{(2)}$, which could allow us to directly identify the nature of the emitting second-order states.

4. CONCLUSIONS

In this article we have described a new multipulse time-resolved fluorescence experiment that is able to isolate and quantify the recombination times of multiexcited states in an ensemble QD sample. Analysis of second-order yields in a sample of CdSe/CdS core/shell QDs enabled us to exclude biexcitons as the source of second-order emission. Furthermore, calculation of *N*th pulse emission intensities allowed us to explore several models of QD recombination dynamics, which indicated that radiative recombination from charged QDs is a likely explanation for the second-order emission.

We envisage that this multipulse time-resolved fluorescence method will be a useful tool in the study and analysis of second-order fluorescence in QDs. The ability to distinguish different sources of second-order emission could enhance our understanding of multiexciton dynamics and the effects of particle charging on QD photophysics. In combination with single particle fluorescence these measurements could yield a clearer picture of QD fluorescence blinking.

The strength of this technique lies in its ability to resolve small second-order fluorescence contributions, which, in turn, relies on the ability to control both pulse energy and pulse number. This extra dimension enables us to collect decay series that can be globally analyzed using the formalisms described here, effectively increasing the signal-to-noise ratio far beyond what is possible if the only tunable parameter is pulse energy. We can run experiments with a wide range of pulse numbers and energies, and we are currently extending the electronics to enable a prespecified pulse series to be collected automatically. Further studies are currently underway to use this technique to explore multiexcited state dynamics in a much wider range of systems.

■ ASSOCIATED CONTENT

Supporting Information

(1) A full derivation of the equations used for data analysis; (2) A description of how absorption cross sections and the average number of excitation events per pulse were estimated; (3) A derivation of functions that describe the probability of generating different QD excitation populations; (4) The procedure for estimating average lifetime uncertainties; (5) A list of the parameters used to fit the fluorescence decays; and (6) A list of the 5- and 7-state scheme parameters used to fit the $j_N^{(2)}$ intensities. This material is available free of charge via the Internet at http://pubs.acs.org.

■ AUTHOR INFORMATION

Corresponding Author

*E-mail: marcus.jones@uncc.edu.

Author Contributions

The manuscript was written through contributions of all authors. All authors have given approval to the final version of the manuscript.

Notes

The authors declare no competing financial interest.

■ ACKNOWLEDGMENTS

M.J. acknowledges startup support from UNC Charlotte.

■ REFERENCES

(1) Alivisatos, A. Semiconductor Clusters, Nanocrystals, and Quantum Dots. *Science* **1996**, *271*, 933−937.

(2) Efros, A. L.; Rosen, M. The Electronic Structure of Semiconductor Nanocrystals. *Annu. Rev. Mater. Sci.* **2000**, *30*, 475−521.
(3) Nozik, A. J. Nanoscience and Nanostructures for Photovoltaics and Solar Fuels. *Nano Lett.* **2010**, *10*, 2735−2741.
(4) Koleilat, G. I.; Levina, L.; Shukla, H.; Myrskog, S. H.; Hinds, S.; Pattantyus-Abraham, A. G.; Sargent, E. H. Efficient, Stable Infrared Photovoltaics Based on Solution-Cast Colloidal Quantum Dots. *ACS Nano* **2008**, *2*, 833−840.
(5) Steckel, J. S.; Snee, P.; Coe-Sullivan, S.; Zimmer, J. P.; Halpert, J. E.; Anikeeva, P.; Kim, L.-A.; Bulovic, V.; Bawendi, M. G. Color-Saturated Green-Emitting QD-LEDs. *Angew. Chem., Int. Ed.* **2006**, *45*, 5796−5799.
(6) Dang, C.; Lee, J.; Breen, C.; Steckel, J. S.; Coe-Sullivan, S.; Nurmikko, A. Red, Green and Blue Lasing Enabled by Single-Exciton Gain in Colloidal Quantum Dot Films. *Nat. Nano.* **2012**, *7*, 335−339.
(7) Brokmann, X.; Giacobino, E.; Dahan, M.; Hermier, J. P. Highly Efficient Triggered Emission of Single Photons by Colloidal CdSe/ZnS Nanocrystals. *Appl. Phys. Lett.* **2004**, *85*, 712−714.
(8) Pisanello, F.; Leménager, G.; Martiradonna, L.; Carbone, L.; Vezzoli, S.; Desfonds, P.; Cozzoli, P. D.; Hermier, J.-P.; Giacobino, E.; Cingolani, R.; et al. Non-Blinking Single-Photon Generation with Anisotropic Colloidal Nanocrystals: Towards Room-Temperature, Efficient, Colloidal Quantum Sources. *Adv. Mater.* **2013**, *25*, 1974−1980.
(9) Puzzo, D. P.; Henderson, E. J.; Helander, M. G.; Wang, Z.; Ozin, G. A.; Lu, Z. Visible Colloidal Nanocrystal Silicon Light-Emitting Diode. *Nano Lett.* **2011**, *11*, 1585−1590.
(10) Kwak, J.; Bae, W. K.; Lee, D.; Park, I.; Lim, J.; Park, M.; Cho, H.; Woo, H.; Yoon, D. Y.; Char, K.; et al. Bright and Efficient Full-Color Colloidal Quantum Dot Light-Emitting Diodes Using an Inverted Device Structure. *Nano Lett.* **2012**, *12*, 2362−2366.
(11) Nozik, A. Spectroscopy and Hot Electron Relaxation Dynamics in Semiconductor Quantum Wells and Quantum Dots. *Annu. Rev. Phys. Chem.* **2001**, *52*, 193−231.
(12) Wong, C. Y.; Kim, J.; Nair, P. S.; Nagy, M. C.; Scholes, G. D. Relaxation in the Exciton Fine Structure of Semiconductor Nanocrystals. *J. Phys. Chem. C* **2009**, *113*, 795−811.
(13) Kambhampati, P. Hot Exciton Relaxation Dynamics in Semiconductor Quantum Dots: Radiationless Transitions on the Nanoscale. *J. Phys. Chem. C* **2011**, *115*, 22089−22109.
(14) Cho, B.; Peters, W. K.; Hill, R. J.; Courtney, T. L.; Jonas, D. M. Bulklike Hot Carrier Dynamics in Lead Sulfide Quantum Dots. *Nano Lett.* **2010**, *10*, 2498−2505.
(15) Salvador, M. R.; Graham, M. W.; Scholes, G. D. Exciton-Phonon Coupling and Disorder in the Excited States of CdSe Colloidal Quantum Dots. *J. Chem. Phys.* **2006**, *125*, 184709.
(16) Madrid, A. B.; Hyeon-Deuk, K.; Habenicht, B. F.; Prezhdo, O. V. Phonon-Induced Dephasing of Excitons in Semiconductor Quantum Dots: Multiple Exciton Generation, Fission, and Luminescence. *ACS Nano* **2009**, *3*, 2487−2494.
(17) Kambhampati, P. Unraveling the the Structure and Dynamics of Excitons in Semiconductor Quantum Dots. *Acc. Chem. Res.* **2011**, *44*, 1−13.
(18) Munro, A. M.; Jen-LaPlante, I.; Ng, M. S.; Ginger, D. S. Quantitative Study of the Effects of Surface Ligand Concentration on CdSe Nanocrystal Photoluminescence. *J. Phys. Chem. C* **2007**, *111*, 6220−6227.
(19) Williams, E. S.; Major, K. J.; Tobias, A.; Woodall, D.; Morales, V.; Lippincott, C.; Moyer, P. J.; Jones, M. Characterizing the Influence of TOPO on Exciton Recombination Dynamics in Colloidal CdSe Quantum Dots. *J. Phys. Chem. C* **2013**, *117*, 4227−4237.
(20) Frederick, M. T.; Weiss, E. A. Relaxation of Exciton Confinement in CdSe Quantum Dots by Modification with a Conjugated Dithiocarbamate Ligand. *ACS Nano* **2010**, *4*, 3195−3200.
(21) Jones, M.; Lo, S. S.; Scholes, G. D. Quantitative Modeling of the Role of Surface Traps in CdSe/CdS/ZnS Nanocrystal Photoluminescence Decay Dynamics. *Proc. Natl. Acad. Sci. U.S.A.* **2009**, *106*, 3011−3016.
(22) Beard, M. C. Multiple Exciton Generation in Semiconductor Quantum Dots. *J. Phys. Chem. Lett.* **2011**, *2*, 1282−1288.
(23) Cunningham, P. D.; Boercker, J. E.; Foos, E. E.; Lumb, M. P.; Smith, A. R.; Tischler, J. G.; Melinger, J. S. Enhanced Multiple Exciton Generation in Quasi-One-Dimensional Semiconductors. *Nano Lett.* **2011**, *11*, 3476−3481.
(24) Jaeger, H. M.; Fischer, S.; Prezhdo, O. V. The Role of Surface Defects in Multi-Exciton Generation of Lead Selenide and Silicon Semiconductor Quantum Dots. *J. Chem. Phys.* **2012**, *136*, 064701.
(25) Zohar, G.; Baer, R.; Rabani, E. Multiexciton Generation in IV−VI Nanocrystals: the Role of Carrier Effective Mass, Band Mixing, and Phonon Emission. *J. Phys. Chem. Lett.* **2013**, *4*, 317−322.
(26) Sukhovatkin, V.; Hinds, S.; Brzozowski, L.; Sargent, E. H. Colloidal Quantum-Dot Photodetectors Exploiting Multiexciton Generation. *Science* **2009**, *324*, 1542−1544.
(27) Nair, G.; Chang, L.-Y.; Geyer, S. M.; Bawendi, M. G. Perspective on the Prospects of a Carrier Multiplication Nanocrystal Solar Cell. *Nano Lett.* **2011**, *11*, 2145−2151.
(28) Hillhouse, H. W.; Beard, M. C. Solar Cells From Colloidal Nanocrystals: Fundamentals, Materials, Devices, and Economics. *Curr. Opin. Colloid Interface* **2009**, *14*, 245−259.
(29) Hanna, M. C.; Nozik, A. J. Solar Conversion Efficiency of Photovoltaic and Photoelectrolysis Cells with Carrier Multiplication Absorbers. *J. Appl. Phys.* **2006**, *100*, 074510.
(30) Semonin, O. E.; Luther, J. M.; Choi, S.; Chen, H.-Y.; Gao, J.; Nozik, A. J.; Beard, M. C. Peak External Photocurrent Quantum Efficiency Exceeding 100% via MEG in a Quantum Dot Solar Cell. *Science* **2011**, *334*, 1530−1533.
(31) Kambhampati, P. Multiexcitons in Semiconductor Nanocrystals: a Platform for Optoelectronics at High Carrier Concentration. *J. Phys. Chem. Lett.* **2012**, *3*, 1182−1190.
(32) Oron, D.; Kazes, M.; Banin, U. Multiexcitons in Type-II Colloidal Semiconductor Quantum Dots. *Phys. Rev. B* **2007**, *75*, 035330.
(33) Htoon, H.; Malko, A. V.; Bussian, D.; Vela, J.; Chen, Y.; Hollingsworth, J. A.; Klimov, V. I. Highly Emissive Multiexcitons in Steady-State Photoluminescence of Individual "Giant" CdSe/CdS Core/Shell Nanocrystals. *Nano Lett.* **2010**, *10*, 2401−2407.
(34) Huxter, V. M.; Scholes, G. D. Nonlinear Optical Approach to Multiexciton Relaxation Dynamics in Quantum Dots. *J. Chem. Phys.* **2006**, *125*, 144716.
(35) Klimov, V.; Mikhailovsky, A.; Xu, S.; Malko, A.; Hollingsworth, J.; Leatherdale, C.; Eisler, H.; Bawendi, M. G. Optical Gain and Stimulated Emission in Nanocrystal Quantum Dots. *Science* **2000**, *290*, 314−317.
(36) Klimov, V. I. Mechanisms for Photogeneration and Recombination of Multiexcitons in Semiconductor Nanocrystals: Implications for Lasing and Solar Energy Conversion. *J. Phys. Chem. B* **2006**, *110*, 16827−16845.
(37) Muller, A.; Fang, W.; Lawall, J.; Solomon, G. S. Creating Polarization-Entangled Photon Pairs From a Semiconductor Quantum Dot Using the Optical Stark Effect. *Phys. Rev. Lett.* **2009**, *103*, 217402.
(38) Stevenson, R. M.; Young, R. J.; Atkinson, P.; Cooper, K.; Ritchie, D. A.; Shields, A. J. A Semiconductor Source of Triggered Entangled Photon Pairs. *Nature* **2006**, *439*, 179−182.
(39) Klimov, V. I. Spectral and Dynamical Properties of Multilexcitons in Semiconductor Nanocrystals. *Annu. Rev. Phys. Chem.* **2007**, *58*, 635−673.
(40) Frantsuzov, P.; Kuno, M.; Janko, B.; Marcus, R. A. Universal Emission Intermittency in Quantum Dots, Nanorods and Nanowires. *Nat. Phys.* **2008**, *4*, 519−522.
(41) Galland, C.; Ghosh, Y.; Steinbrück, A.; Sykora, M.; Hollingsworth, J. A.; Klimov, V. I.; Htoon, H. Two Types of Luminescence Blinking Revealed by Spectroelectrochemistry of Single Quantum Dots. *Nature* **2011**, *479*, 203−207.
(42) Dahan, M.; Lévi, S.; Luccardini, C.; Rostaing, P.; Riveau, B.; Triller, A. Diffusion Dynamics of Glycine Receptors Revealed by Single-Quantum Dot Tracking. *Sci. Signaling* **2003**, *302*, 442−445.

(43) Courty, S.; Luccardini, C.; Bellaiche, Y.; Cappello, G.; Dahan, M. Tracking Individual Kinesin Motors in Living Cells Using Single Quantum-Dot Imaging. *Nano Lett.* **2006**, *6*, 1491−1495.
(44) Zhao, J.; Bardecker, J. A.; Munro, A. M.; Liu, M. S.; Niu, Y.; Ding, I.-K.; Luo, J.; Chen, B.; Jen, A. K. Y.; Ginger, D. S. Efficient CdSe/CdS Quantum Dot Light-Emitting Diodes Using a Thermally Polymerized Hole Transport Layer. *Nano Lett.* **2006**, *6*, 463−467.
(45) Michler, P.; Imamoğlu, A.; Mason, M. D.; Carson, P. J.; Strouse, G. F.; Buratto, S. K. Quantum Correlation Among Photons From a Single Quantum Dot at Room Temperature. *Nature* **2000**, *406*, 968−970.
(46) Klimov, V. I. Spectral and Dynamical Properties of Multiexcitons in Semiconductor Nanocrystals. *Annu. Rev. Phys. Chem.* **2007**, *58*, 635−673.
(47) Schaller, R. D.; Sykora, M.; Jeong, S.; Klimov, V. I. High-Efficiency Carrier Multiplication and Ultrafast Charge Separation in Semiconductor Nanocrystals Studied via Time-Resolved Photoluminescence. *J. Phys. Chem. B* **2006**, *110*, 25332−25338.
(48) Klimov, V. I. Optical Nonlinearities and Ultrafast Carrier Dynamics in Semiconductor Nanocrystals. *J. Phys. Chem. B* **2000**, *104*, 6112−6123.
(49) Nair, G.; Bawendi, M. G. Carrier Multiplication Yields of CdSe and CdTe Nanocrystals by Transient Photoluminescence Spectroscopy. *Phys. Rev. B* **2007**, *76*, 081304.
(50) Guyot-Sionnest, P.; Wehrenberg, B.; Yu, D. Intraband Relaxation in CdSe Nanocrystals and the Strong Influence of the Surface Ligands. *J. Chem. Phys.* **2005**, *123*, 074709.
(51) Gabriel, M. M.; Grumstrup, E. M.; Kirschbrown, J. R.; Pinion, C. W.; Christesen, J. D.; Zigler, D. F.; Cating, E. E. M.; Cahoon, J. F.; Papanikolas, J. M. Imaging Charge Separation and Carrier Recombination in Nanowire P-I-N Junctions Using Ultrafast Microscopy. *Nano Lett.* **2014**, *14*, 3079−3087.
(52) Lo, S. S.; Devadas, M. S.; Major, T. A.; Hartland, G. V. Optical Detection of Single Nano-Objects by Transient Absorption Microscopy. *Analyst* **2012**, *138*, 25−31.
(53) Jones, M.; Scholes, G. D. On the Use of Time-Resolved Photoluminescence as a Probe of Nanocrystal Photoexcitation Dynamics. *J. Mater. Chem.* **2010**, *20*, 3533−3538.
(54) Korkusinski, M.; Voznyy, O.; Hawrylak, P. Fine Structure and Size Dependence of Exciton and Biexciton Optical Spectra in CdSe Nanocrystals. *Phys. Rev. B* **2010**, *82*, 245304.
(55) Sewall, S. L.; Franceschetti, A.; Cooney, R. R.; Zunger, A.; Kambhampati, P. Direct Observation of the Structure of Band-Edge Biexcitons in Colloidal Semiconductor CdSe Quantum Dots. *Phys. Rev. B* **2009**, *80*, 081310.
(56) Mcguire, J. A.; Sykora, M.; Joo, J.; Pietryga, J. M.; Klimov, V. I. Apparent Versus True Carrier Multiplication Yields in Semiconductor Nanocrystals. *Nano Lett.* **2010**, *10*, 2049−2057.
(57) Nair, G.; Geyer, S. M.; Chang, L.-Y.; Bawendi, M. G. Carrier Multiplication Yields in PbS and PbSe Nanocrystals Measured by Transient Photoluminescence. *Phys. Rev. B* **2008**, *78*, 125325.
(58) Shabaev, A.; Hellberg, C. S.; Efros, A. L. Efficiency of Multiexciton Generation in Colloidal Nanostructures. *Acc. Chem. Res.* **2013**, *46*, 1242−1251.
(59) Nair, G.; Zhao, J.; Bawendi, M. G. Biexciton Quantum Yield of Single Semiconductor Nanocrystals From Photon Statistics. *Nano Lett.* **2011**, *11*, 1136−1140.
(60) Efros, A.; Rosen, M.; Kuno, M.; Nirmal, M.; Norris, D.; Bawendi, M. G. Band-Edge Exciton in Quantum Dots of Semiconductors with a Degenerate Valence Band: Dark and Bright Exciton States. *Phys. Rev. B* **1996**, *54*, 4843−4856.
(61) Jones, M.; Lo, S. S.; Scholes, G. D. Signatures of Exciton Dynamics and Carrier Trapping in the Time-Resolved Photoluminescence of Colloidal CdSe Nanocrystals. *J. Phys. Chem. C* **2009**, *113*, 18632−18642.
(62) Salman, Al. A.; Tortschanoff, A.; Van Der Zwan, G.; van Mourik, F.; Chergui, M. A Model for the Multi-Exponential Excited-State Decay of CdSe Nanocrystals. *Chem. Phys.* **2009**, *357*, 96−101.
(63) van Driel, A. F.; Nikolaev, I. S.; Vergeer, P.; Lodahl, P.; Vanmaekelbergh, D.; Vos, W. L. Statistical Analysis of Time-Resolved Emission From Ensembles of Semiconductor Quantum Dots: Interpretation of Exponential Decay Models. *Phys. Rev. B* **2007**, *75*, 035329.
(64) Zhang, J.; Zhang, X.; Zhang, J. Y. Size-Dependent Time-Resolved Photoluminescence of Colloidal CdSe Nanocrystals. *J. Phys. Chem. C* **2009**, *113*, 9512−9515.
(65) Kippeny, T. C.; Bowers, M. J.; Dukes, A. D.; McBride, J. R.; Orndorff, R. L.; Garrett, M. D.; Rosenthal, S. J. Effects of Surface Passivation on the Exciton Dynamics of CdSe Nanocrystals as Observed by Ultrafast Fluorescence Upconversion Spectroscopy. *J. Chem. Phys.* **2008**, *128*, 084713.
(66) Osad'ko, I. S. Distribution of Photons in Single Quantum Dot Intermittent Photoluminescence with Power-Law Distribution of on/Off Intervals. *J. Phys. Chem. C* **2013**, *117*, 11328−11336.
(67) Efros, A.; Rosen, M. Random Telegraph Signal in the Photoluminescence Intensity of a Single Quantum Dot. *Phys. Rev. Lett.* **1997**, *78*, 1110−1113.
(68) Zhao, J.; Nair, G.; Fisher, B. R.; Bawendi, M. G. Challenge to the Charging Model of Semiconductor-Nanocrystal Fluorescence Intermittency From Off-State Quantum Yields and Multiexciton Blinking. *Phys. Rev. Lett.* **2010**, *104*, 157403.
(69) Ye, M.; Searson, P. C. Blinking in Quantum Dots: the Origin of the Grey State and Power Law Statistics. *Phys. Rev. B* **2011**, *84*, 125317.
(70) Park, Y. S.; Malko, A. V.; Vela, J.; Chen, Y.; Ghosh, Y.; García-Santamaría, F.; Hollingsworth, J. A.; Klimov, V. I.; Htoon, H. Near-Unity Quantum Yields of Biexciton Emission From CdSe/CdS Nanocrystals Measured Using Single-Particle Spectroscopy. *Phys. Rev. Lett.* **2011**, *106*, 187401.
(71) Bacher, G.; Weigand, R.; Seufert, J.; Kulakovskii, V.; Gippius, N.; Forchel, A.; Leonardi, K.; Hommel, D. Biexciton Versus Exciton Lifetime in a Single Semiconductor Quantum Dot. *Phys. Rev. Lett.* **1999**, *83*, 4417−4420.
(72) Califano, M.; Franceschetti, A.; Zunger, A. Lifetime and Polarization of the Radiative Decay of Excitons, Biexcitons, and Trions in CdSe Nanocrystal Quantum Dots. *Phys. Rev. B* **2007**, *75*, 115401.
(73) Taguchi, S.; Saruyama, M.; Teranishi, T.; Kanemitsu, Y. Quantized Auger Recombination of Biexcitons in CdSe Nanorods Studied by Time-Resolved Photoluminescence and Transient-Absorption Spectroscopy. *Phys. Rev. B* **2011**, *83*, 155324.
(74) Saba, M.; Aresti, M.; Quochi, F.; Marceddu, M.; Loi, M. A.; Huang, J.; Talapin, D. V.; Mura, A.; Bongiovanni, G. Light-Induced Charged and Trap States in Colloidal Nanocrystals Detected by Variable Pulse Rate Photoluminescence Spectroscopy. *ACS Nano* **2013**, *7*, 229−238.
(75) Clapp, A. R.; Goldman, E. R.; Mattoussi, H. Capping of CdSe-ZnS Quantum Dots with DHLA and Subsequent Conjugation with Proteins. *Nat. Protoc.* **2006**, *1*, 1258−1266.
(76) Li, J.; Wang, Y.; Guo, W.; Keay, J.; Mishima, T.; Johnson, M.; Peng, X. Large-Scale Synthesis of Nearly Monodisperse CdSe/CdS Core/Shell Nanocrystals Using Air-Stable Reagents via Successive Ion Layer Adsorption and Reaction. *J. Am. Chem. Soc.* **2003**, *125*, 12567−12575.
(77) van Embden, J.; Jasieniak, J.; Gomez, D. E.; Mulvaney, P.; Giersig, M. Review of the Synthetic Chemistry Involved in the Production of Core/Shell Semiconductor Nanocrystals. *Aust. J. Chem.* **2007**, *60*, 457−471.
(78) O'Connor, D. V.; Phillips, D. *Time-Correlated Single Photon Counting*; Academic Press: New York, 1984.
(79) Leatherdale, C.; Woo, W.; Mikulec, F.; Bawendi, M. G. On the Absorption Cross Section of CdSe Nanocrystal Quantum Dots. *J. Phys. Chem. B* **2002**, *106*, 7619−7622.
(80) Zhao, J.; Chen, O.; Strasfeld, D. B.; Bawendi, M. G. Biexciton Quantum Yield Heterogeneities in Single CdSe (CdS) Core (Shell) Nanocrystals and Its Correlation to Exciton Blinking. *Nano Lett.* **2012**, *12*, 4477−4483.

(81) Liu, Y. S.; Ware, W. R. Photophysics of Polycyclic Aromatic-Hydrocarbons Adsorbed on Silica-Gel Surfaces 0.1. Fluorescence Lifetime Distribution Analysis - an Ill-Conditioned Problem. *J. Phys. Chem.* **1993**, *97*, 5980−5986.
(82) LeBlanc, S. J.; McClanahan, M. R.; Jones, M.; Moyer, P. J. Enhancement of Multiphoton Emission From Single CdSe Quantum Dots Coupled to Gold Films. *Nano Lett.* **2013**, *13*, 1662−1669.
(83) Mcguire, J. A.; Sykora, M.; Robel, I.; Padilha, L. A.; Joo, J.; Pietryga, J. M.; Klimov, V. I. Spectroscopic Signatures of Photocharging Due to Hot-Carrier Transfer in Solutions of Semiconductor Nanocrystals Under Low-Intensity Ultraviolet Excitation. *ACS Nano* **2010**, *4*, 6087−6097.
(84) Krauss, T. D.; Peterson, J. J. Bright Future for Fluorescence Blinking in Semiconductor Nanocrystals. *J. Phys. Chem. Lett.* **2010**, *1*, 1377−1382.
(85) Lupo, M. G.; Sala, D. F.; Carbone, L.; Zavelani-Rossi, M.; Fiore, A.; Lüer, L.; Polli, D.; Cingolani, R.; Manna, L.; Lanzani, G. Ultrafast Electron−Hole Dynamics in Core/Shell CdSe/CdS Dot/Rod Nanocrystals. *Nano Lett.* **2008**, *8*, 4582−4587.
(86) Rainò, G.; Stoeferle, T.; Moreels, I.; Gomes, R.; Kamal, J. S.; Hens, Z.; Mahrt, R. F. Probing the Wave Function Delocalization in CdSe/CdS Dot-in-Rod Nanocrystals by Time- and Temperature-Resolved Spectroscopy. *ACS Nano* **2011**, *5*, 4031−4036.
(87) Luo, J.-W.; Franceschetti, A.; Zunger, A. Carrier Multiplication in Semiconductor Nanocrystals: Theoretical Screening of Candidate Materials Based on Band-Structure Effects. *Nano Lett.* **2008**, *8*, 3174−3181.
(88) Fernee, M. J.; Littleton, B. N.; Rubinsztein-Dunlop, H. Detection of Bright Trion States Using the Fine Structure Emission of Single CdSe/ZnS Colloidal Quantum Dots. *ACS Nano* **2009**, *3*, 3762−3768.